9.11 EVALUATION OF TEMPORAL AND SPATIAL DISTRIBUTION OF TAMDAR DATA IN SHORT-RANGE MESOSCALE FORECASTS

Neil A. Jacobs[1*], Yubao Liu[2], and Cyrena-Marie Druse[1]

[1]AirDat, LLC, Morrisville, NC 27560
[2]National Center for Atmospheric Research, Boulder, CO 80307

1. INTRODUCTION AND MOTIVATION

Upper-air observations are disproportionately sparse, both temporally and geographically, when compared to surface observations. The lack of data is likely one of the largest limiting factors in numerical weather prediction.

Atmospheric measurements performed by the Tropospheric Airborne Meteorological Data Reporting (TAMDAR) sensor of humidity, pressure, temperature, winds aloft, icing, and turbulence, along with the corresponding location, time, and altitude from built-in GPS are relayed via satellite in real-time to a ground-based network operations center. The TAMDAR sensors are deployed on a fleet of 63 Saab 340s operated by Mesaba Airlines in the Great Lakes region as a part of the NASA-sponsored Great Lakes Fleet Experiment (GLFE). More than 800 soundings are generated from 400 flights to 75 regional airports during a 24-h period.

A two-part case study is conducted using the 22-23 April 2005 cyclogenetic event over the Great Lakes region. A mesoscale model using real-time four-dimensional data assimilation is employed to draw comparisons from parallel short-range simulations where the experimental (control) run includes (withholds) TAMDAR data. The second part of this study varies the vertical resolution by increasing the number of model σ-levels from 36 to 48. Over half of the additional σ-levels are added to the lowest 1.5 km. This is done for both the control and experimental simulations for the same 22-23 April 2005 case. In the last part, a quantitative precipitation forecast (QPF) verification study is conducted on multiple numerical weather models using the 22-23 April 2005 case. An objective precipitation cell isolation technique is employed to quantify the accuracy of each model with respect to magnitude and location of precipitation cells.

The objectives of this study are to (i) identify impacts that TAMDAR data may have on mesoscale model forecasts by increasing the horizontal distribution of vertical atmospheric profiles during initialization, and (ii) to isolate the model's ability to utilize higher vertical data resolution; thus quantifying any impacts it may have for this particular case.

Corresponding author address: Neil A. Jacobs, AirDat, LLC, 2400 Perimeter Park Dr. Suite 100, Morrisville, NC 27560. Email: njacobs@airdat.com

2. CASE BACKGROUND

Multiple cold fronts passed through the Great Lakes region beginning on 20 April 2005. On 22 April, a large upper-level trough moved across the same region. A strong surface low pressure formed along the frontal boundary in conjunction with this trough. By 1800 UTC 22 April, downstream blocking began to decrease the forward progression of the now cutoff upper-level low. Phasing between the surface and upper-level low caused the surface low pressure to retrograde westward as it strengthened to below 986 mb. Record snowfall amounts exceeding 12 in. were reported in southeast Michigan, while strong winds and blowing snow resulted in drifts more than 4 ft. high.

This case occurred just after the entire Mesaba fleet switched over to the high-resolution pressure ascent mode. During this time, TAMDARs recorded observations every 10 hPa for the first 200 hPa (approximately the 800-hPa level), and the descent mode recorded observations every 10 hPa for the lowest 100 hPa. Above this zone, observations were recorded every 50 hPa.

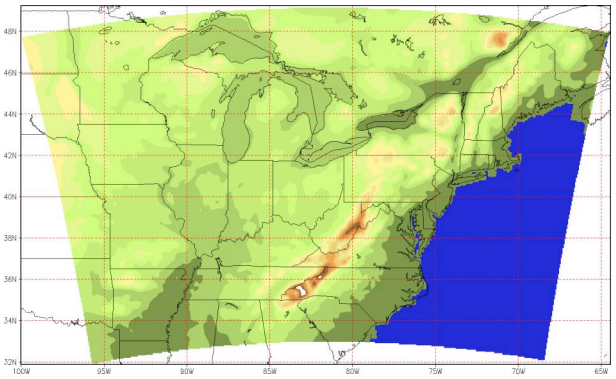

Fig. 1. The Lambert Conformal grid for the domain to which all model (and Stage-IV analysis) precipitation forecasts are regridded.

3. METHODOLOGY AND MODEL CONFIGURATION

The models tested in this study are the NCAR/AirDat mesoscale model with a real-time four-dimensional data assimilation system (RT-FDDA-MM5) to process Tropospheric Airborne Meteorological Data Reporting (TAMDAR) observations, the North American Mesoscale Model-218 (NAM218, aka. Eta), the Rapid Update

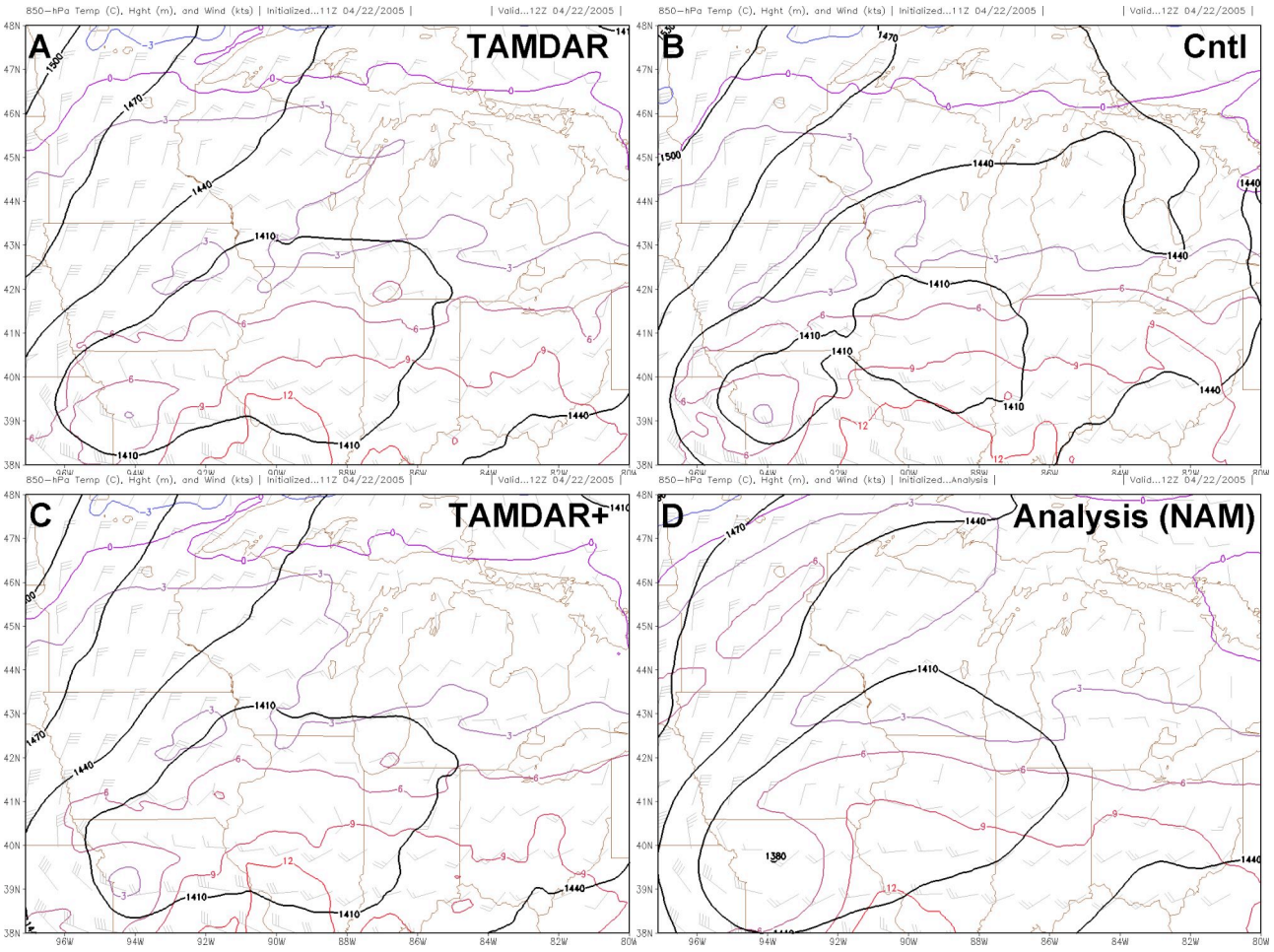

Fig. 2. The 850-hPa temperatures (C), heights (m), and winds (kts) valid 1200 UTC 22 April 2005 for the TAMDAR (A), Cntl (B), and the TAMDAR+ (C) 1-h forecasts, as well as the NAM-218 analysis (D).

Cycle-13 (RUC13), and the Global Forecast System (GFS, aka. AVN/MRF). The GFS is projected on a spectral triangular 254 domain and transformed to a 768x384 grid with approximately 0.5-degree spacing (e.g., Kanamitsu 1989; Kanamitsu et al. 1991; and Kalnay et al. 1990). NCEP's NAM-218 employs 12-km grid spacing for a CONUS Lambert Conformal of 614x428 (e.g., Black 1994; Gartner et al. 1998; and Rogers et al. 2001). Both the GFS and the NAM-218 are run at 00Z, 06Z, 12Z, and 18Z. The RUC13 has the same CONUS domain as the RUC20, but at 13-km (451x337) grid spacing. Forecasts for 12 hours are generated on a 3-h cycle beginning at 00Z (Benjamin et al. 2004; 2004a; and 2004b).

The NCAR/AirDat RT-FDDA system is built around the Fifth Generation of the Penn State/National Center for Atmospheric Research (PSU/NCAR) Mesoscale Model (MM5, Grell et al. 1994). There are currently 2 nested domains of 36-km and 12-km grid spacing centered over the Great Lakes region. The 12-km grid is 213x147. A continuous data ingestion system using Newtonian relaxation is utilized to generate an analysis period to bring the model to geostrophic balance. This method greatly reduces the time and errors associated with typical model spin-up (Stauffer and Seaman 1994; Cram et al. 2001; Davis et al. 1999; and Liu et al. 2002). The NCAR/AirDat RT-FDDA is run on a 3-h cycle much like that used by RUC13; however, the cycle times are ahead by 1 hour (i.e., 23Z, 2Z, 5Z, 8Z, 11Z, 14Z, 17Z, and 20Z). This means that the NCAR/AirDat model forecast is 1 hour further in the future when comparing all the model forecast outputs at 00Z, 06Z, 12Z, and 18Z. This is an inherent disadvantage for the NCAR/AirDat model not accounted for in the results.

Although RT-FDDA is a cycling data ingestion style system, for the purposes of domain manipulation within this study, the MM5 was cold-started with RT-FDDA generated analysis fields, thus it does not include the standard continuous observation assimilation during the first 2 forecast hours. Standard INTERPF and MM5 were run on a separate system for all simulations. The four simulations will be referred to as TAMDAR, TAMDAR+, Cntl, and Cntl +. The TAMDAR and Cntl simulations both have 36 σ-levels, and the TAMDAR+ and Cntl+ both have 48 σ-levels. The additional 12 σ-levels appear within the

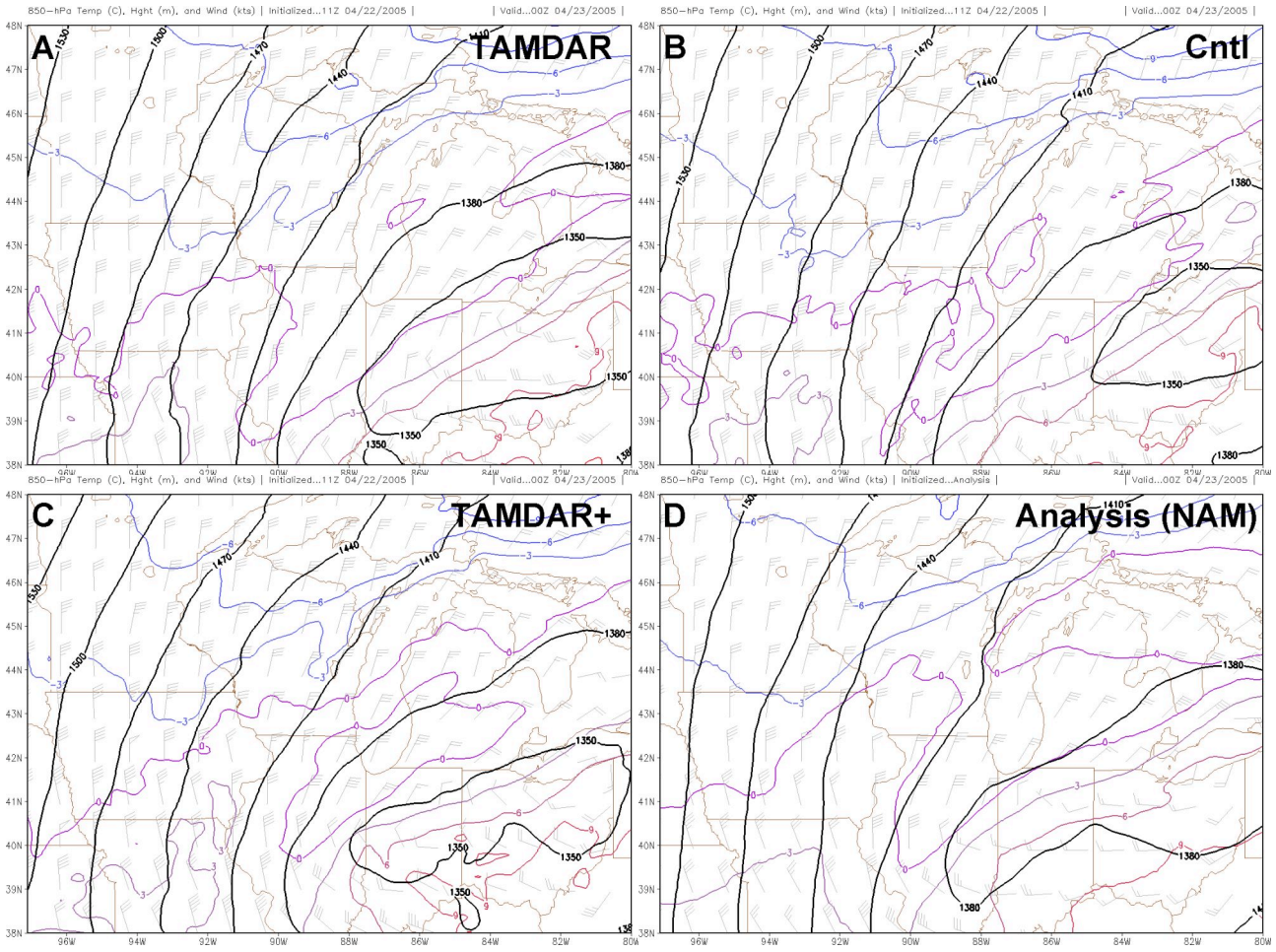

Fig. 3. The 850-hPa temperatures (C), heights (m), and winds (kts) valid 0000 UTC 23 April 2005 for the TAMDAR (A), Cntl (B), and the TAMDAR+ (C) 13-h forecasts, as well as the NAM-218 analysis (D).

lowest 5.5 km, and 6 of those 12 σ-levels reside in the lowest 1.5 km. This spacing was chosen to best utilize the increased observation density provided by the TAMDARs. The remaining model parameters were left unchanged. Like the operational RT-FDDA-MM5, there are two nested domains of 36-km and 12-km grid spacing. The 12-km domain is shown in Fig. 1. The Grell cumulus parameterization was chosen for its handling of convective precipitation at smaller grid scales. The MRF planetary boundary layer scheme, as well as the Mixed-phase (Reisner-1) microphysics were also chosen to be consistent with the analysis field generation methods. All simulations were initialized 1100 UTC 22 April 2005, and were run for 14 h. Comparisons with other various government models below are conducted against the 1200 UTC 22 April 2005 runs after the various model forecasts are interpolated to the same 12-km grid of 213x147 seen in the terrain representation for the domain in Fig. 1.

Stage-IV multi-sensor precipitation estimator (MPE) is mosaicked into national 4-km coverage of Stage-II data after it has been passed through a manual quality control process. The Stage-II merged radar estimated rainfall and gauge data is real-time, hourly, multi-sensor National Precipitation Analysis (NPA) developed by NCEP and the Office of Hydrology (Fulton et al. 1998; Seo 1998; and Seo et al. 1999). For verification purposes, the Stage-IV data is assumed to be the "truth", thus it is treated as the QPF control for this study.

Historical model outputs and forecast data (not including the NCAR/AirDat forecast data) were obtained through NCDC's NOMADS[1] archive.

4. SENSITIVITY TO VERTICAL RESOLUTION

The 850-hPa temperatures, heights, and winds are shown in Fig. 2, which is valid 1200 UTC 22 April, a 1-h forecast for the simulations. There are minimal differences between the TAMDAR run (Fig. 2A) and the TAMDAR+ run (Fig. 2C). Both the TAMDAR and TAMDAR+ runs are also in agreement with the NAM-218 analysis (Fig. 2D), valid for the same time. However, height differences between the Cntl (Fig. 2B) and the

[1] http://nomads.ncdc.noaa.gov/

other simulations, as well as the analysis, are already evident. The differences in temperature are less significant at this point. Figure 3, valid 0000 UTC 23 April, is 13 h into the simulation period. By this time, the Cntl has veered further from the truth, while the TAMDAR simulations, which are still in fairly good agreement, more closely resemble the analysis. Although there are differences in the 850-hPa temperatures, the most notable feature is the attempt, made by the Cntl (Fig. 3B), to accelerate the motion of the low pressure eastward. This is not seen in the TAMDAR (Fig. 3A) or the TAMDAR+ (Fig. 3C). It should be noted here that the NAM-218 forecast (not shown), which was initialized with the analysis seen in Fig. 3D, generated large downstream errors by accelerating the low too fast to the east. These errors, apparent as early as 0300 UTC 23 April, bring the validity of the 0000 UTC 23 April analysis into question. Large errors in 2-m temperatures (> 5°C) in the 0000 UTC 23 April NAM-218 analysis were also noted when compared against station observations throughout Illinois and Indiana.

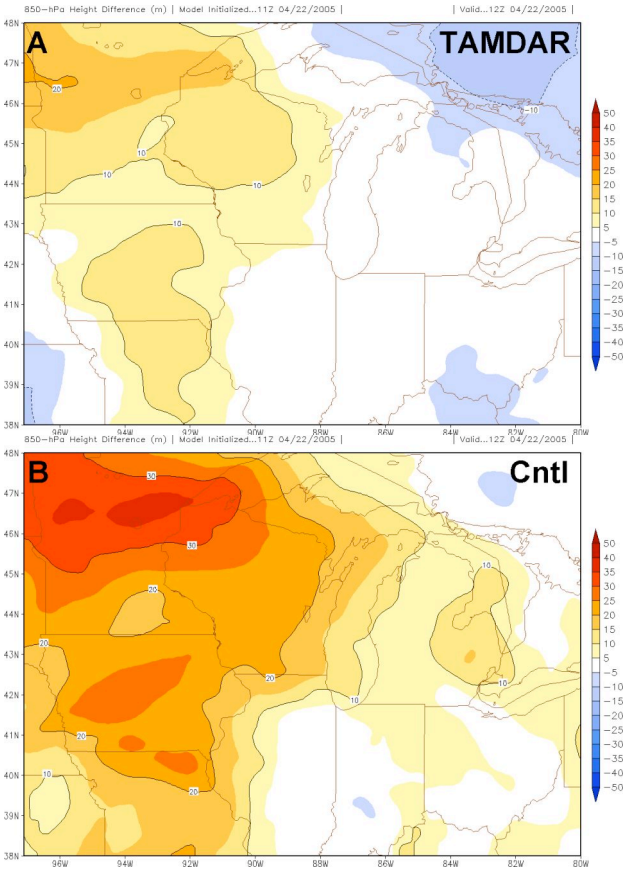

Fig. 4. The 850-hPa height difference (m) between the TAMDAR (A), or Cntl (B), 1-h forecast, valid 1200 UTC 22 April, and the 1200 UTC 22 April NAM-218 analysis.

A difference field between the simulations and the NAM-218 analysis of 850-hPa heights (Fig. 4), valid 1200 UTC 22 April (1-h forecast), suggests that the initial errors began as the Cntl (Fig. 4B) failed to properly initialize the depth of the trough entering from the west. This error is still evident 6 h later (1800 UTC 22 April), as seen in Fig. 5B. The source of the elevated heights in Fig. 5B is a result of the eastward progression being too fast, which is consistent with the motion of the low seen in Fig 3B. The central low pressure at the 850-hPa level in both simulations (Fig. 5) is much deeper than the NAM-218 analysis. However, the comparison in Fig. 5, which is valid 1800 UTC 22 April, is generated with an analysis field containing limited, if any, reliable upper-level observations.

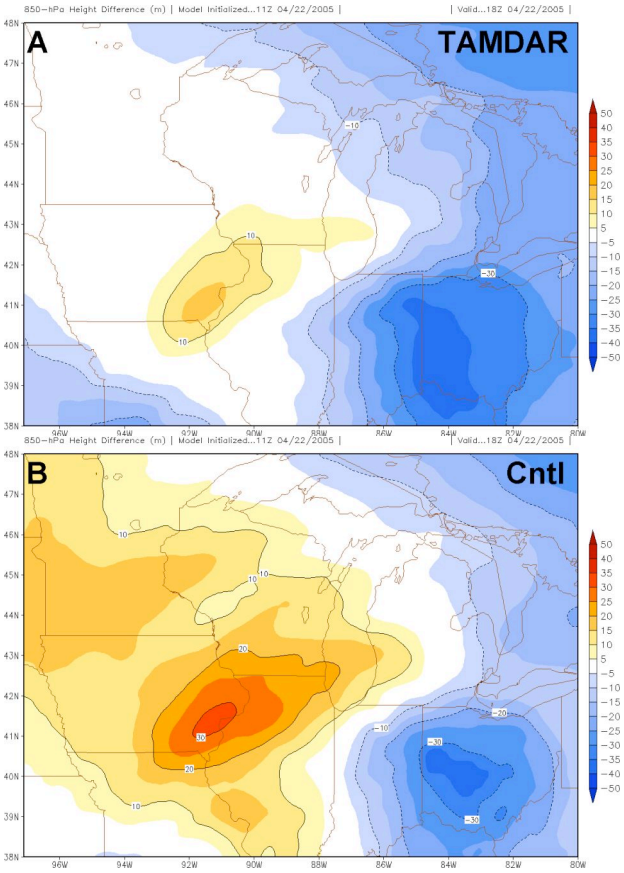

Fig. 5. The 850-hPa height difference (m) between the TAMDAR (A), or Cntl (B), 7-h forecast, valid 1800 UTC 22 April, and the 1800 UTC 22 April NAM-218 analysis.

A comparison of 1-h precipitation, valid 1200 UTC 22 April, is seen in Fig. 6. Both TAMDAR (Fig. 6A) and the Cntl (Fig. 6B) capture the general precipitation region. The TAMDAR appears to better resolve the cells located over northern Indiana, while the Cntl more closely represents the two-line feature entering Iowa (cf. Fig. 6D). Both TAMDAR and Cntl over-predict precipitation in the region directly north and east of the area of central low pressure along the Indiana and Illinois border. The TAMDAR+ (Fig. 6C) produces a much more accurate representation of the precipitation features when compared to the Stage-IV analysis (Fig. 6D). The region over Indiana, down to individual bands, is captured very well, as is the parallel-line feature in the western region

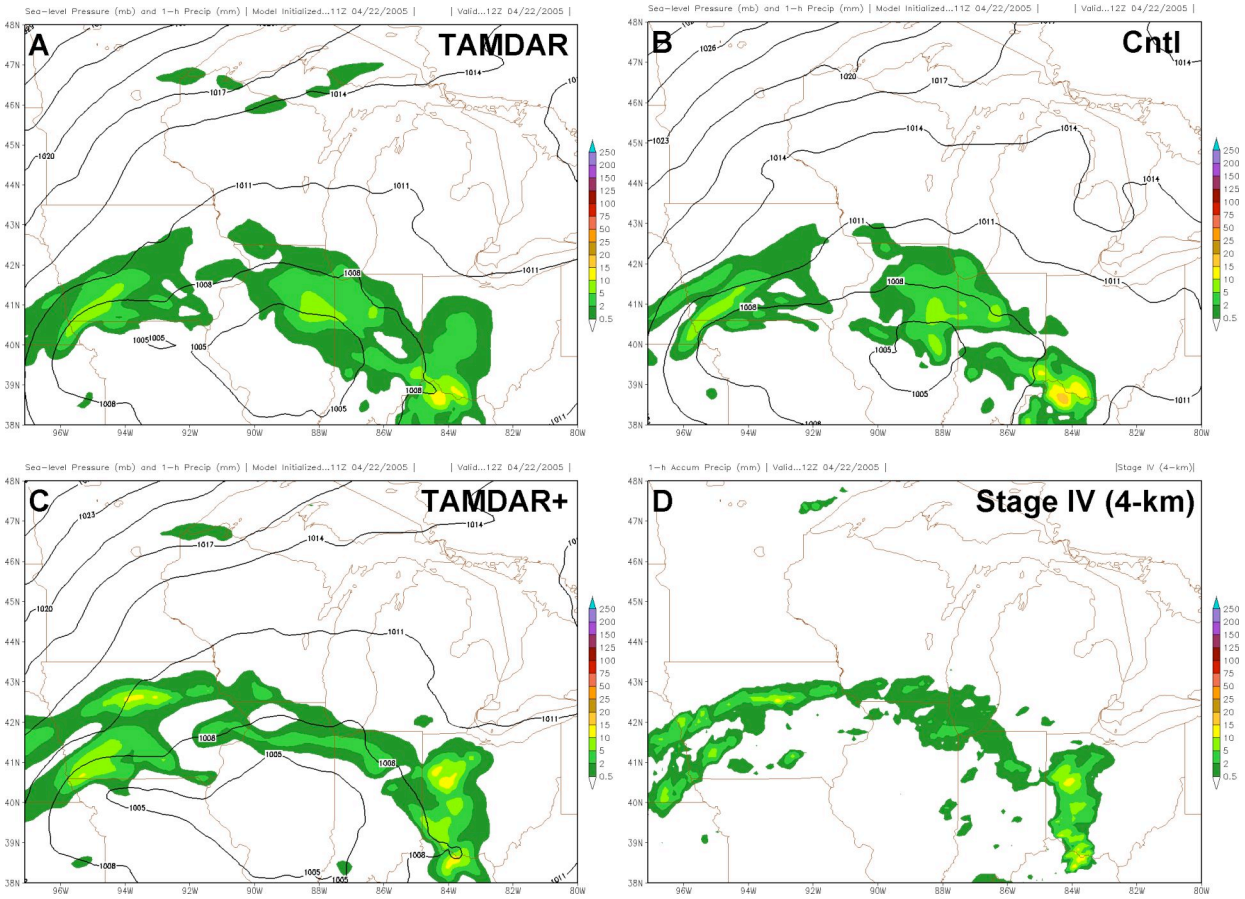

Fig. 6. The 1-h precipitation forecast (mm) and sea-level pressure (mb) for TAMDAR (A), Cntl (B), and TAMDAR+ (C), as well as the 1-h Stage-IV analysis (mm), valid 1200 UTC 22 April 2005.

on the plot. The TAMDAR+ also performs better by damping convection in the region northeast of the surface low pressure where the other runs over-predicted amounts of precipitation.

Similar results were found when comparing other model-generated parameters such as vorticity and relativity humidity. Additional comparisons of the fields discussed above for various levels between the surface and 500 hPa were also performed; however, the largest differences are seen in the layers surrounding the 850-hPa level.

5. PRECIPITATION CELL ISOLATION

This study began with a simple point by point comparison to gauge the models QPF performance using observations from selected cities to verify rainfall totals. It became evident that the major limitation of this method would be the lack of ability to quantify the model's error. According to preliminary results, the model would score a complete "bust" if it correctly predicted the magnitude of a thunderstorm cell, but missed the location (of the analysis/observation) by as little as 1 grid point, or forecasted no precipitation in the entire domain. Although, both would be considered incorrect, the latter is much further from the truth. The odds of a model correctly forecasting the exact amount of precipitation for every grid point in the domain are quite low, thus the initial methods were altered to include quantification of the forecast error.

In order to compare various model forecasts on a per precipitation cell basis, the precipitation cells must be isolated from each other, as well as background noise (e.g., convective feedback, etc.). The inherent chaotic shape of frontal banding features and thunderstorm cells warrants a complex filtering program to sort the cells. The idea is to isolate particular cells based on their maximum magnitude of precipitation, yet retain all the lower values of precipitation directly associated with that cell. A simple program to search for maximum values wound not work because it would eliminate all lesser values whether they were associated with the cell in question, or not. To overcome this concern, the revised code is designed to first seek out precipitation cell maxima based on a pre-defined threshold. For this study, thresholds of 5 mm to 40 mm, in increments of 5 mm, were chosen. Once the cell is identified, the program conducts a radial search following the gradient until it reaches a pre-defined minimum value (both 2 and 5 mm were used). A second order derivative is used to detect

the cell edges. This Laplacian edge detection method uses discrete difference approximations to estimate the derivatives, and represent the Laplacian of function f(x,y) as

$$\nabla^2 f(x,y) = \frac{\partial^2 f(x,y)}{\partial x^2} + \frac{\partial^2 f(x,y)}{\partial y^2}. \qquad (1)$$

After the precipitation cells, and their associated values of lesser precipitation are isolated/identified, other cells below the threshold of interest are eliminated.

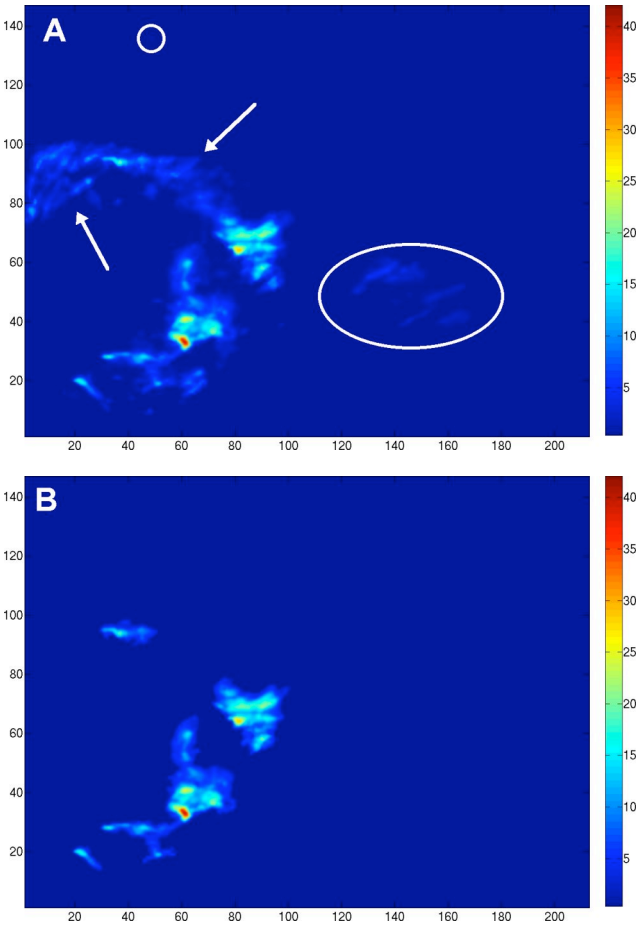

Fig. 7. The raw Stage-IV 3-h accumulated precipitation data (A), and the postprocessed 20-mm (5 mm minimum) isolated cells (B) valid 1500 UTC 22 April 2005. The domain-2 data are mapped on the x-y grid. The white arrows and circles in (A) highlight features that are eliminated in (B).

Examples of this procedure are seen in Fig. 7A and Fig. 7B. Figure 7A is raw Stage-IV 3-h accumulated precipitation data valid 1500 UTC 22 April 2005. The x and y-axis are grid points from the domain seen in Fig. 1. The white arrows and circles highlight features that are eliminated in the example process of this technique. The result from the isolation of cells with maxima greater than, or equal to, 20 mm is shown in Fig. 7B. A lower bound of 5 mm was imposed for this edge detection example; however, for the statistical comparison discussed later, results were obtained using a lower boundary of 2 mm because the 5-mm lower boundary was found to be too limiting.

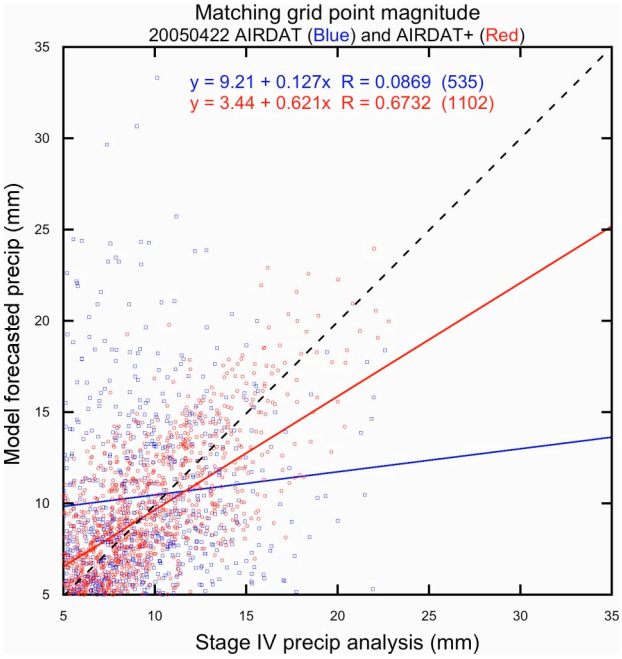

Fig. 8. Scatter plot of 1-h QPF totals versus the 1-h Stage-IV analysis comparing matching grid point magnitudes (above 5 mm threshold) summed over each of the 14 forecast hours. The TAMDAR (AIRDAT) is blue, and the TAMDAR+ (AIRDAT+) is red.

The matching grid point magnitudes summed over the forecast period are shown in Fig. 8 and Fig. 9 for all values above the 5 mm threshold. The plots show 1-h QPF totals versus the 1-h Stage-IV analysis for each of the 14 forecast hours. In both Fig. 8 and Fig. 9, the TAMDAR (AIRDAT) and Cntl (AIRNOT) are blue, while the TAMDAR+ (AIRDAT+) and Cntl+ (AIRNOT+) are shown in red. Linear regression fits appear for each data set in the respective color. As mentioned above, the odds of correctly forecasting the precipitation magnitude in each model grid point are highly unlikely, so it is not surprising that the regression fits suggest that the data is nothing more than noise. However, the TAMDAR+ run more than doubles the number of matching data (535 to 1102 points) over the TAMDAR run (Fig. 8). In addition to this, an extensive improvement in correlation, which increases the explained variance more than 40%, is seen.[2] The data for the Cntl (AIRNOT) and Cntl+ are shown in Fig. 9. The Cntl+ run increases the number of matching data by about 30%, but the correlation between these data only improves the explained variance by 4%

[2] Although the results here are quite impressive, more cases must be analyzed before this degree of improvement can be considered a trend.

over the Cntl (AIRNOT). It is also worth noting that the Cntl (AIRNOT) run shows greater correlation than the TAMDAR run; however, it also has fewer data points. Regardless, both coefficients in the Cntl runs are very low.

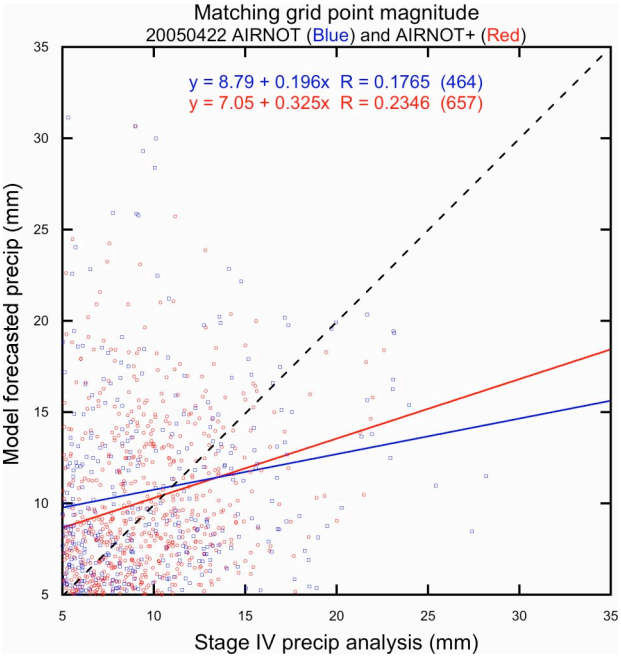

Fig. 9. Scatter plot of 1-h QPF totals versus the 1-h Stage-IV analysis comparing matching grid point magnitudes (above 5 mm threshold) summed over each of the 14 forecast hours. The Cntl (AIRNOT) is blue, and the Cntl+ (AIRNOT+) is red.

6. PRECIPITATION FORECAST COMPARISON

To gauge the space-time accuracy of the models QPF per cell. A weighting scheme was applied to each grid point with a non-zero magnitude of precipitation. The weighting is a linear multiplier, which is dynamically derived from the radius of the cell's maximum value grid point to the edge of the minimum bound. This was conducted in eight x-y orientations (e.g., 0,1; 1,1; 1,0; 1,-1; 0,-1; -1,-1; -1,0; -1,1), and applied to the difference field between the regridded model forecast and the Stage-IV analysis. The regridded Stage-IV data is still considered "truth", thus the difference field between itself yields zero (i.e., no weighting scheme is applied). An example of the precipitation cell forecast comparison is shown in Fig. 10, valid 0000 UTC 23 April 2005. The weighted grid point value scores, which are essentially the magnitudes of the precipitation at the grid points times the linear multipliers, for various model's 12-h forecasts, as well as the Stage-IV analysis, are shown for the isolation of 20-mm cells. In Fig. 10, maximum values between 2 and 10 mm are seen. This is because the perimeter of the cell covers more area than the core of the cell, thus it covers more grid points as well. For isolated cells greater than 5 mm (not shown), all the models, except the GFS, performed quite well. There is a noticeable over-prediction in precipitation magnitude, which is likely an artifact of convective feedback from cumulus (or convective) parameterization (CP) schemes in the models (Grell 1993). This primarily appears as noise in lower thresholds (<15 mm). In addition to this, Stage-IV is not entirely error free. Although it is used as the control because it is generally accepted as "truth", it has minor biases, which are typically dry (e.g., Groisman 1994; Nespor; and Sevruk 1999). There have been significant advancements in gauge correcting algorithms (Seo 1998; Seo et al. 1999), so it is taken here as the best precipitation analysis option for a control. Notable differences between the models begin to arise (seen first in the 6-h forecast, not shown) with the isolation of 15-mm cells. Beyond the 20 mm threshold (Fig. 10), the differences are significant, as the models (not including TAMDAR+) fail to capture the most intense precipitation. It should be noted here that the AIRNOT+ forecast (No TAMDAR with increased σ-levels) produced results similar to the TAMDAR and Cntl (AIRNOT) results in Fig. 10.

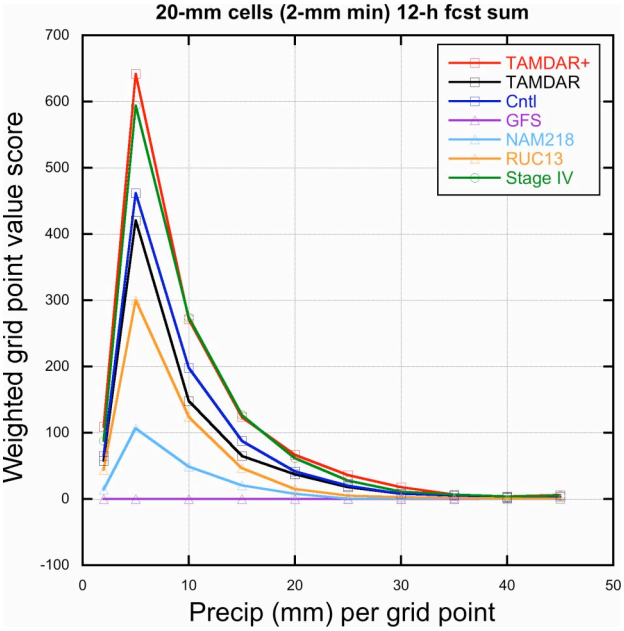

Fig. 10. Comparison of 12-h QPF between TAMDAR+, TAMDAR, Cntl, GFS, NAM-218, and RUC13, as well as the Stage-IV analysis (control) for 20-mm cells with 2-mm minimum bound.

7. CONCLUSIONS

Results suggest that the addition of TAMDAR data improves the experimental simulation for certain output parameters. Additionally, when increasing the vertical resolution, results show significant improvements through the 12-h experimental simulation for parameters such as geopotential height, temperature, and winds from the surface level to above the 500-hPa level. The most notable improvements when increasing the number of model σ-levels occur between the 900-hPa and 800-hPa

level. Results also suggest that more accurate lower and mid-tropospheric model initializations feed back to the surface, thus improving sea-level pressure and 10-m wind fields, as well as quantitative precipitation forecasts.

The NCAR/AirDat model runs for TAMDAR and the Cntl both show improvements in 3-h QPF over various government models from 50% at a cell threshold of 15 mm to greater than 80% for cells larger than 30 mm. However, these results are largely due to the advanced ingestion technique of the RT-FDDA system.[3] When the statistics for all precipitation cell sizes are summed for the 22 April 2005 case, the improvements of TAMDAR over the Cntl are about 5%. The variance from bin to bin, depending on the cell size, was between 2% and 12% for this case, thus the improvements are statistically indistinguishable. However, the TAMDAR+ run shows significant improvements of 18-22% over the TAMDAR, Cntl, and the Cntl+ (AIRNOT), as well as improvements of 50-90% over other various government models.

8. ACKNOWLEDGMENTS

The authors would like to thank Stan Benjamin and William Moninger (NOAA/ERL/FSL) for their comments and suggestions on this work. The authors are very grateful for the computer support provided by NCAR. We would like to acknowledge the NASA Aeronautics Research Office's Aviation Safety Program, the FAA Aviation Weather Research Program, and AirDat, LLC for their support in this effort.

9. REFERENCES

Benjamin, S.G., T.G. Smirnova, K.J. Brundage, S.S. Weygandt, D. Devenyi, B.E. Schwartz, T.L. Smith, 2004: Application of the Rapid Update Cycle at 10-13 km - Initial testing. *Preprints 16th Conf. Num. Wea. Pred.,* Seattle, WA, Amer. Meteor. Soc., CD-ROM, 8.3.

Benjamin, S.G., D. Devenyi, S.S. Weygandt, K.J. Brundage, J.M. Brown, G.A. Grell, D. Kim, B.E. Schwartz, T.G. Smirnova, T.L. Smith, and G.S. Manikin, 2004a: An hourly assimilation/forecast cycle: The RUC. *Mon. Wea. Rev.* ,132, 495-518.

Benjamin, S.G., G.A. Grell, J.M. Brown, T.G. Smirnova, and R. Bleck, 2004b: Mesoscale weather prediction with the RUC hybrid isentropic / terrain-following coordinate model. *Mon. Wea. Rev.* ,**132**, 473-494.

Black, T. L., 1994: The new NMC Mesoscale Eta model: Description and forecast examples. *Wea. Forecasting*, **9**, 265-278.

Cram, J. M., Y. Liu, S. Low-Nam, R-S. Sheu, L. Carson, C. A. Davis, T. Warner, J. F. Bowers, 2001: An operational mesoscale RT-FDDA analysis and forecasting system. *Preprints 18th WAF and 14th NWP Confs*., Ft. Lauderdale, AMS, Boston, MA.

Davis, C., T. Warner, E. Astling, and J. Bowers, 1999: Development and application of an operational, relocatable, mesogamma-scale weather analysis and forecasting system. Tellus, 51A, 710-727.

Fulton, R.A., J.P. Breidenbach, D.J. Seo, D.A. Miller, and T. O'Bannon, 1998: The WSR-88D rainfall algorithm. *Wea. and Fore.,***13,** 377-395.

Gartner, W. E., M. E. Baldwin, and N. W. Junker, 1998: Regional analysis of quantitative precipitation forecasts from NCEP's Early Eta and Meso-Eta models. Preprints, *16th Conf. on Weather Analysis and Forecasting*, Phoenix, AZ, Amer. Meteor. Soc., 187-189.

Grell, G. A., 1993: Prognostic evaluation of assumptions used by cumulus parameterizations. *Mon. Wea. Rev.*, **121**, 764-787.

Grell, G. A., J. Dudhia, and D. R. Stauffer, 1994: A description of the Fifth-Generation Penn State/NCAR Mesoscale Model (MM5). NCAR Tech. Note NCAR/TN-398+STR,122 pp.

Groisman, P. Ya., and D. R. Legates, 1994: The accuracy of United States precipitation data. *Bull. Amer. Meteor. Soc.*, **75**, 215-227.

Kalnay, M. Kanamitsu, and W.E. Baker, 1990: Global numerical weather prediction at the National Meteorological Center. Bull. Amer. Meteor. Soc., 71, 1410-1428.

Kanamitsu, M., 1989: Description of the NMC global data assimilation and forecast system. Wea. and Forecasting, 4, 335-342.

Kanamitsu, M., J.C. Alpert, K.A. Campana, P.M. Caplan, D.G. Deaven, M. Iredell, B. Katz, H.-L. Pan, J. Sela, and G.H. White, 1991: Recent changes implemented into the global forecast system at NMC. Wea. and Forecasting, 6, 425-435.

Nespor, V., and B. Sevruk, 1999: Estimation of wind-induced error of rainfall gauge measurements using a numerical simulation. *J. Atmos. Oceanic Technol.*, **16**, 450- 464.

Rogers, E., M. Ek, Y. Lin. K. Mitchell, D. Parrish, and G. DiMego, 2001 : Changes to the NCEP Meso Eta Analysis and Forecast System: Assimilation of observed precipitation, upgrades to land-surface physics, modified 3DVAR analysis. NWS Technical Procedures Bulletin No.479. [Available from the National Weather Service, Office of Meteorology, 1325 East-West Highway, Silver Spring, MD 20910].

[3] The results presented here are consistent with preliminary findings from similar studies conducted at NCAR.

Seo, D.J., 1998: Real-time estimation of rainfall fields using radar rainfall and rain gauge data. *J. of Hydrol.,* **208,** 37-52.

Seo, D.J., J.P. Breidenbach, and E.R. Johnson, 1999: Real-time estimation of mean field bias in radar rainfall data. *J. of Hydrol.,* **209,** 131-147.

Stauffer, D. R., and N. L. Seaman, 1994: Multiscale four-dimensional data assimilation. *J. Appl. Meteor*., 33, 416-434.

Liu, Y., S. Low-Nam, R. Sheu, L. Carson, C. Davis, T. Warner, S. Swerdlin, J. Bowers, M. Xu, H-M Hsu, and D. Rife, 2002: Performance and Enhancement of the NCAR/ATEC mesoscale FDDA and forecast system. 15th Conference on Numerical Weather Prediction, 12-16 August, 2002, San Antonio, Taxes, 399-402.